Acoustic nonlinearity parameter induced by extended dislocations

Xiang Gao and Jianmin Qu[a)]

Department of Mechanical Engineering, Tufts University, Medford, Massachusetts 02155, USA

Excess acoustic nonlinearity is a signature of microstructural defects on a propagating ultrasound. By measuring the excess acoustic nonlinearity parameter, defect characteristics can be inferred nondestructively through ultrasonic techniques. To this end, proper models are needed to relate the excess acoustic nonlinearity parameter with defect characteristics. In this study, an analytical model for extended dislocations is developed that relates the excess acoustic nonlinearity parameter with characteristics of the extended dislocation including dislocation density, stacking fault energy, and equilibrium distance between the two partial dislocations that form the extended dislocation. According to this model, the excess acoustic nonlinearity parameter induced by extended dislocations consists of a stress-independent term and a stress-dependent term. Both terms are scaled with $(L_{char}/b)^n$, where L_{char} is the equilibrium distance between the two partials, b is the magnitude of Burgers vector, and n is 3 and 4 for the stress-independent and stress-dependent terms, respectively. The model will be useful for interpreting results from ultrasonic nondestructive evaluation of material defects. *Published by AIP Publishing.* https://doi.org/10.1063/1.5046640

I. INTRODUCTION

Dislocations often control the mechanical behaviors of crystalline solids. Knowing the density of dislocations and their substructures is critical in determining the mechanical properties of materials such as yield strength and fatigue life. In recent years, nondestructive evaluation (NDE) techniques based on nonlinear ultrasound have been developed[1–11] to characterize material defects such as dislocations. A directly measurable quantity through nonlinear ultrasonic test is the acoustic nonlinearity parameter (ANLP), which is related to the defects that cause the acoustic nonlinearity. Therefore, in order to use nonlinear ultrasound as an NDE technique to characterize dislocations, a quantitative relationship that relates the ANLP to dislocation characteristics (such as density, Burgers vector, characteristic lengths, etc.) needs to be developed.

Acoustic nonlinearity in crystalline solids comes from two sources. One is lattice anharmonicity which is manifested by the third order elastic constants. The other is microstructural defects which interact with the propagating wave in a nonlinear fashion. The anharmonicity-induced acoustic nonlinearity is considered intrinsic to the perfect lattice, while the defect-induced acoustic nonlinearity is considered excess over and above the intrinsic acoustic nonlinearity in that it exists only when certain defects are present. In other words, the total ANLP of the medium may be written as

$$\beta = \beta^{lat} + \beta^{dis}, \qquad (1)$$

where β^{lat} and β^{dis} represent the intrinsic and excess ANLPs, respectively.

First, we consider the intrinsic acoustic nonlinearity. For elastic solids with quadratic nonlinearity, the one-

dimensional stress-strain relation in the *x*-direction can be expressed through the first Piola-Kirchhoff stress

$$\sigma = E_2 \frac{\partial u}{\partial x} + \frac{1}{2} E_3 \left(\frac{\partial u}{\partial x} \right)^2 + \cdots, \qquad (2)$$

where u is the particle displacement and E_2 and E_3 are the second- and third-order Huang's coefficients,[12] respectively. By substituting Eq. (2) into the equation of motion and neglecting higher order terms, one obtains the following one-dimensional nonlinear wave equation for the particle displacement

$$\frac{1}{c^2} \frac{\partial^2 u}{\partial t^2} - \frac{\partial^2 u}{\partial x^2} = -\beta^{lat} \frac{\partial u}{\partial x} \frac{\partial^2 u}{\partial x^2}, \qquad (3)$$

where c is the phase velocity of the wave and $\beta^{lat} = -E_3/E_2$ is the intrinsic ANLP.

As a sinusoidal plane wave of frequency ω propagates through this nonlinear elastic medium, second harmonic is generated by the intrinsic acoustic nonlinearity. Through a straightforward perturbation technique,[13,14] an asymptotic solution to Eq. (3) can be written as follows by neglecting higher order terms,

$$u(x, t) = A \sin \left[\omega \left(t - \frac{x}{c} \right) \right]$$
$$+ \beta^{lat} \frac{A^2 \omega^2 x}{8c^2} \cos \left[2\omega \left(t - \frac{x}{c} \right) \right] + \cdots, \qquad (4)$$

where A is the amplitude of the fundamental wave. It is seen from this solution that the amplitude of the second harmonic is proportional to the intrinsic ANLP, which can then be obtained experimentally by carrying the Fourier transform of the time domain signal in the received ultrasonic wave. This is the basic principle on which many nonlinear ultrasonic NDE techniques are based. Equation (4) also implies that second harmonic is the sole ramification of the acoustic nonlinearity in the solids.

[a)]Author to whom correspondence should be addressed: jianmin.qu@tufts.edu

In addition to the lattice anharmonicity, crystalline solids often contain microstructural defects such as dislocations. As an ultrasonic wave propagates through the solid, it interacts with the defects. Such interactions are often nonlinear, which gives rise to the excess acoustic nonlinearity. The excess acoustic nonlinearity, according to the foregoing discussion, will generate additional second harmonic. Consequently, for a plane wave propagating in a solid with defects, it follows from Eq. (4) that the displacement will be in the form of

$$u(x, t) = A \sin\left[\omega\left(t - \frac{x}{c}\right)\right]$$
$$+ (\beta^{lat} + \beta^{dis})\frac{A^2\omega^2 x}{8c^2}\cos\left[2\omega\left(t - \frac{x}{c}\right)\right] + \cdots, \quad (5)$$

where β^{dis} is the excess ANLP induced by dislocations. Since the total ANLP $\beta = \beta^{lat} + \beta^{dis}$ can be measured experimentally by conducting nonlinear ultrasonic tests as discussed earlier, and β^{lat} is known to be $-E_3/E_2$, one may then conclude that the excess ANLP β^{dis} can be measured experimentally by conducting nonlinear ultrasonic tests. Thus, if a quantitative relationship can be established between β^{dis} and the characteristics of the defects, one may obtain quantitative information about the defects inside the medium by measuring β^{dis} via ultrasonic tests, which is important in determining the mechanical properties of the solids and monitoring the health conditions of the structures. This is the basic idea, on which nonlinear ultrasonic techniques for nondestructive evaluation of defects are based.

Clearly, the key point for developing nonlinear ultrasonic NDE techniques for defect characterization is to establish the relationship between the excess ANLP β^{dis} and the characteristics of defects. The types of defects that have been considered in the existing literature include dislocations,[15–19] precipitates,[20–23] and microcracks.[24–27]

In this work, we focus on dislocations. Hikata et al.[15,16] were the first to investigate a segment of dislocation line pinned at its two ends by other defects such as precipitates, vacancies, or grain boundaries. Such pinned dislocation segments or monopoles appear often in metallic materials with precipitate strengthening mechanisms.[28,29] Under shear stress, the pinned dislocation segment bows out within its slip plane, which induces shear strain. However, the resulting shear strain is nonlinearly related to the applied shear stress, which gives rise to acoustic nonlinearity. By assuming constant dislocation line tension and elastic isotropy of the solid, Hikata et al.[15] derived a quantitative relationship between β^{dis} and the dislocation characteristics, such as dislocation density, segment length, Burgers vectors, etc. Later, Cash and Cai[18] demonstrated by dislocation dynamics simulations that constant dislocation line tension is insufficient to capture the correct behavior of acoustic nonlinearity and proposed a revised model that considers the orientation-dependence of dislocation line tension. Extending Cash and Cai,[18] Chen and Qu[17] further studied the effects of mixed dislocations and elastic anisotropy.

Another defect structure is dislocation dipole, which consists of two edge dislocations of opposite signs located on two different slip planes separated by an atomic distance. These two edge dislocations maintain a stable equilibrium state under their mutual interactions. Dislocation dipoles appear often in engineering materials. For example, cyclic loading in metal fatigue promotes the formation of dislocation dipoles.[30] Cantrell and Yost[31] first developed an analytical model for the excess ANLP caused by dislocation dipoles. In their model, only the stress-independent part of the excess ANLP is captured. Later, Cash and Cai[19] showed, by dislocation dynamics simulations, that the excess ANLP has a significant dependence on the pre-stress. They subsequently improved the original model of Cantrell and Yost[31] and introduced a stress-dependent term in the excess ANLP.

In addition to dislocation monopoles and dipoles, another common dislocation structure is partial dislocations. Under certain conditions, a dislocation may find it energetically favorable to split into two partial dislocations. Simultaneously, a stacking fault region is formed between these two partials. In the literature, a region of stacking fault bounded by two partial dislocations on a slip plane is called *an extended dislocation*.[32,33] In an extended dislocation, the two partials are linear defects while the stacking fault is a planar defect. The separation between the partials is stress-dependent according to Byun,[34] implying that extended dislocations may interact with propagating waves. In this study, we will investigate whether such interactions can induce excess acoustic nonlinearity, and if so, how the excess acoustic nonlinearity is related to characteristics of the extended dislocations.

The paper is organized as follows. Section II derives an analytical expression for the excess ANLP induced by extended dislocations. Section III gives an example for numerical estimation and verification of the derived ANLP. Section IV is devoted to comparisons of the present extended dislocation model (EDM) with existing models for dislocation monopoles and dipoles. A summary and some conclusions are given in Sec. V.

II. ANLP CAUSED BY EXTENDED DISLOCATIONS

In this section, we first consider the separation distance between the partial dislocations under an applied stress. To this end, we note that the energy of a dislocation is proportional to the square of the magnitude of its Burgers vector. According to the Frank Rule, a dislocation may find it energetically favorable to split into two dislocations. In crystal with face-centered cubic (FCC) symmetry, a perfect dislocation may dissociate into two Shockley partial dislocations or one Shockley partial dislocation plus a Frank sessile dislocation.[35] During the dissociation of dislocations, a stacking fault region is formed simultaneously between the partial dislocations. Outside this faulted region, the crystal is perfect. The configuration of an extended dislocation is illustrated in Fig. 1, where a perfect dislocation with line vector $\boldsymbol{\xi}$ and Burgers vector $\boldsymbol{b}$ is split into two partial dislocations with line vector $\boldsymbol{\xi}_n$ and Burgers vector $\boldsymbol{b}_n$ with $n = 1, 2$.

The interaction force between these two partials is repulsive and is inversely proportional to the distance between them, while the stacking fault provides a constant attractive force that pulls the two partials together. Thus, in the absence of externally applied forces, the equilibrium distance
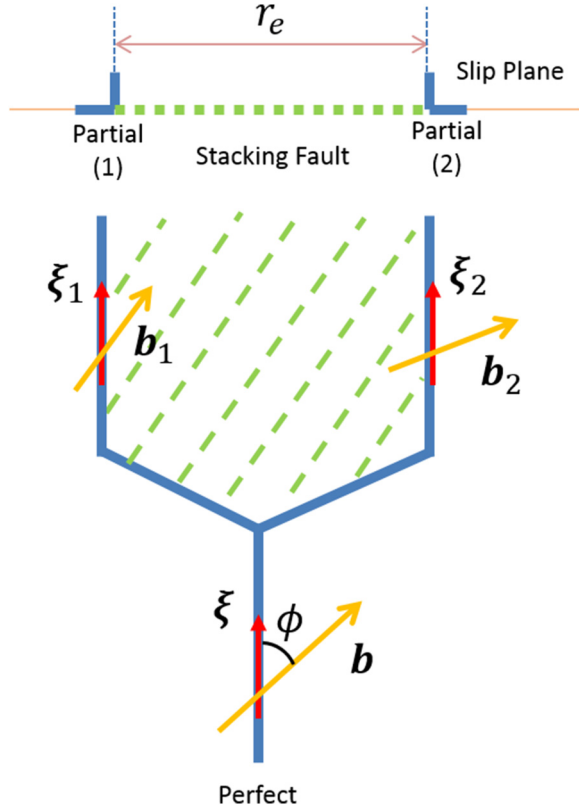
FIG. 1. Configuration of extended dislocations.

FIG. 2. Forces acting on each partial dislocation.

between these two partials is given by

$$r_e = \frac{k}{\gamma},\qquad(6)$$

where γ (J/m^2 or N/m) is the stacking fault energy density and k is a coefficient that characterizes the repulsive force between the two partials. According to Hirth and Lothe,[32] the coefficient k can be expressed as

$$k = \frac{\mu}{2\pi}\left\{(\boldsymbol{b}_1 \cdot \boldsymbol{\xi}_1)(\boldsymbol{b}_2 \cdot \boldsymbol{\xi}_2) + \frac{(\boldsymbol{b}_1 \times \boldsymbol{\xi}_1) \cdot (\boldsymbol{b}_2 \times \boldsymbol{\xi}_2)}{1 - v}\right\},\qquad(7)$$

where μ and v are, respectively, the shear modulus and Poisson's ratio of the solid. In FCC, Burgers vectors of the two Shockley partials share the same magnitude, i.e., $|\boldsymbol{b}_1| = |\boldsymbol{b}_2| = b_p$. Thus, Eq. (7) reduces to[36]

$$k = \frac{\mu b_p^2}{8\pi}\eta, \ \eta = \frac{2 - v}{1 - v}\left(1 - \frac{2v\cos\phi}{2 - v}\right),\qquad(8)$$

where $\phi = \langle \boldsymbol{\xi}, \boldsymbol{b} \rangle$ is the angle between the line vector and the resultant Burger vector of the perfect dislocation.

Since the two partials have different Burgers vectors, they should feel different forces under the same applied stress. Thus, it is perceivable that an applied stress field may change the separation distance from its equilibrium r_e, see Fig. 2. The new separation distance can be written as

$$r_{e,\sigma} = \frac{k}{\gamma + \frac{1}{2}(F_1 - F_2)},\qquad(9)$$

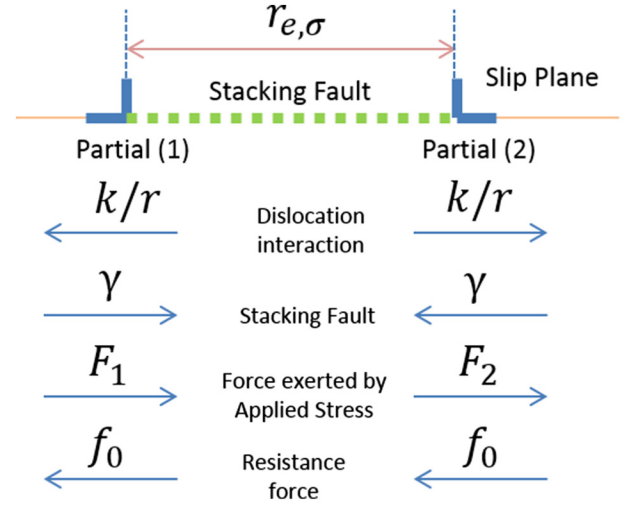where $F_n = C_n\sigma b_p$ for $n = 1, 2$ are the Peach-Koehler

forces[37] exerted on the two partials, respectively. In the above, σ is the applied normal stress and C_n is the conversion factor that converts the local normal stress field to the shear stress in the slip plane. Let $R = (C_2 - C_1)/2$ be the total stress conversion factor. Then, Eq. (9) can be rewritten as

$$r_{e,\sigma} = \frac{k}{\gamma - Rb_p\sigma}.\qquad(10)$$

This is the separation distance between the two partials under the applied normal stress σ.

We are now ready to compute the excess ANLP due to extended dislocations. Assume that the external normal stress σ is applied in the x-direction, the two partials will change their separation distance relative to their equilibrium distance at the stress-free state. Such change can be computed from Eqs. (9) and (10),

$$\Delta r = r_{e,\sigma} - r_e = \frac{k}{\gamma - Rb_p\sigma} - \frac{k}{\gamma}$$

$$= \frac{kRb_p}{\gamma^2}\sigma + \frac{k}{\gamma}\left(\frac{Rb_p}{\gamma}\right)^2\sigma^2 + \frac{k}{\gamma}\left(\frac{Rb_p}{\gamma}\right)^3\sigma^3 + O(\sigma^4).\qquad(11)$$

In deriving the above formula, a Tayler series expansion with respect to σ has been carried out. This change in equilibrium distance between the two partials will induce a shear strain along the slip plane. According to Suzuki, Hikata, and Elbaum[16] and Cantrell and Yost,[31] this shear strain can be written as $\Lambda b_p\Delta r$, where Λ is the density of the extended dislocations. Thus, the deformation gradient corresponding to this shear strain is given by $F^{dis} = 1 + g\Lambda b_p\Delta r$, where g is a conversion factor that converts the dislocation-induced shear strain in the slip plane to the normal strain in the x-direction along which the normal stress is applied.

In addition to the deformation induced by the dislocations, the lattice itself also deforms under the applied stress. This lattice deformation can be represented by the deformation gradient $F^{lat} = 1 + \partial u^{lat}/\partial x$, where $\partial u^{lat}/\partial x$ measures the deformation of the defect-free lattice in the x-direction. Thus, the total deformation gradient under the applied

normal stress is

$$F = 1 + \varepsilon = F^{dis}F^{lat} = (1 + g\Lambda b_p\Delta r)\left(1 + \frac{\partial u^{lat}}{\partial x}\right), \quad (12)$$

where $\varepsilon = \partial u/\partial x$ with u being the actual displacement in the x-direction. For many problems of practical interests, the higher order term in Eq. (12) is negligible. Hence, the total strain is

$$\varepsilon = \frac{\partial u^{lat}}{\partial x} + g\Lambda b_p\Delta r. \quad (13)$$

Without any defects, the stress-strain relation for the lattice follows from Eq. (2). Inverting this equation yields $\partial u^{lat}/\partial x$ as a function of stress σ,

$$\frac{\partial u^{lat}}{\partial x} = \frac{\sigma}{E_2} - \frac{1}{2}\frac{E_3}{E_2^3}\sigma^2 + \frac{1}{2}\frac{E_3^2}{E_2^5}\sigma^3 + O(\sigma^4). \quad (14)$$

Substituting Eq. (14) into (13) in conjunction with (11), and neglecting higher order terms, we obtain

$$\varepsilon = f_1\sigma + f_2\sigma^2 + f_3\sigma^3, \quad (15)$$

where

$$f_1 = \frac{1}{E_2} + \frac{g\Lambda kRb_p^2}{\gamma^2}, f_2 = -\frac{1}{2}\frac{E_3}{E_2^3} + \frac{g\Lambda kR^2b_p^3}{\gamma^3},$$
$$f_3 = \frac{1}{2}\frac{E_3^2}{E_2^5} + \frac{g\Lambda kR^3b_p^4}{\gamma^4}. \quad (16)$$

We note that Eq. (15) gives the constitutive relation for the defective (containing extended dislocations) solids with quadratic nonlinearity. Its inverse can be written as $\sigma = \sigma(\varepsilon)$ where $\sigma(\varepsilon)$ is a smooth function of ε.

Let us now assume that this defective solid is subjected to a pre-stress $\sigma = \sigma_0$, which corresponds to a pre-strain $\varepsilon = \varepsilon_0$. Further, we assume that a wave motion is superimposed on this solid, which generates an additional stress $\Delta\sigma$ and an additional strain $\Delta\varepsilon$. It then follows from Eq. (15) that

$$\Delta\sigma = \left(\frac{d\sigma}{d\varepsilon}\right)_{\varepsilon=\varepsilon_0}\Delta\varepsilon + \frac{1}{2}\left(\frac{d^2\sigma}{d\varepsilon^2}\right)_{\varepsilon=\varepsilon_0}(\Delta\varepsilon)^2 + \cdots, \quad (17)$$

where, following the rules for derivatives of inverse functions,

$$\left(\frac{d\sigma}{d\varepsilon}\right)_{\varepsilon=\varepsilon_0} = \frac{1}{f_1 + 2\sigma_0f_2 + 3\sigma_0^2f_3},$$
$$\left(\frac{d^2\sigma}{d\varepsilon^2}\right)_{\varepsilon=\varepsilon_0} = -\frac{2f_2 + 6\sigma_0f_3}{(f_1 + 2\sigma_0f_2 + 3\sigma_0^2f_3)^3}. \quad (18)$$

Comparison of Eqs. (17) and (2) yields the ANLP,

$$\beta = -\left(\frac{d^2\sigma}{d\varepsilon^2}\right)_{\varepsilon=\varepsilon_0} \bigg/ \left(\frac{d\sigma}{d\varepsilon}\right)_{\varepsilon=\varepsilon_0}$$
$$= \frac{2f_2 + 6\sigma_0f_3}{(f_1 + 2\sigma_0f_2 + 3\sigma_0^2f_3)^2}. \quad (19)$$

Obviously, the ANLP depends on the pre-stress σ_0. The pre-stress σ_0 here is the stress present in the material before the ultrasonic wave is introduced into the material. It may be the

existing residual stress or the stress applied externally. In most practical applications, the pre-stress is very small. Thus, by using series expansion, β can be written as

$$\beta = \beta^{lat} + \beta_0^{dis} + \beta_\sigma^{dis}, \quad (20)$$

where $\beta^{lat} = -E_3/E_2$ is the intrinsic ANLP of the perfect lattice. β_0^{dis} and β_σ^{dis} are, respectively, the stress-independent and stress-dependent parts of the excess ANLP due to the dislocations. Their expressions are given by
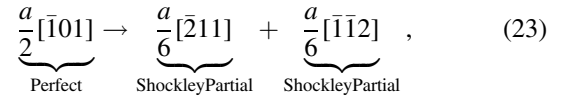
$$\beta_0^{dis} = \frac{E_3}{E_2} + \frac{2f_2}{f_1^2}, \beta_\sigma^{dis} = \left(\frac{6f_3}{f_1^2} - \frac{8f_2^2}{f_1^3}\right)\sigma_0. \quad (21)$$

In most cases, $1/E_2 \gg g\Lambda kRb_p^2/\gamma^2$ which implies that $f_1 \approx 1/E_2$. Thus, Eq. (21) reduces to

$$\beta_0^{dis} = \frac{2E_2^2g\Lambda kR^2b_p^3}{\gamma^3}, \beta_\sigma^{dis} = E_2^2(6f_3 - 8E_2f_2^2)\sigma_0. \quad (22)$$

III. NUMERICAL EXAMPLES

In this section, we will use some typical material properties to estimate the ANLP obtained in Sec. II. Since stacking faults and partial dislocations are often observed experimentally in nickel (Ni), we will use properties of Ni crystal in our numerical analysis. Ni is an FCC crystal where slip occurs on the (111) plane. A perfect dislocation on this plane may dissociate into two Shockley partial dislocations to attain lower energy. Such dislocation dissociation can be represented by the following reaction equation:

$$\underbrace{\frac{a}{2}[\bar{1}01]}_{\text{Perfect}} \rightarrow \underbrace{\frac{a}{6}[\bar{2}11]}_{\text{ShockleyPartial}} + \underbrace{\frac{a}{6}[\bar{1}\bar{1}2]}_{\text{ShockleyPartial}}, \quad (23)$$

where a is the lattice parameter. Its value and other physical parameters are given in Table I.

TABLE I. Physical parameters for estimation of ANLP.

Physical parameters	Symbols	Values	Notes
Lattice parameter	a	3.524×10^{-10} m	
Burgers vector	b_p	1.44×10^{-10} m	$b_p = a/\sqrt{6}$
Stack fault energy	γ	90 mJ/m²[a]	
Poisson's ratio	v	0.31	
2nd order elastic constants	λ	109 GPa[b]	
	μ	81.7 GPa[b]	
3rd order elastic constants	l	−56 GPa[b]	
	m	−671 GPa[b]	
	n	−785 GPa[b]	
1D elastic modulus	E_2	272.4 GPa	$E_2 = \lambda + 2\mu$
	E_3	−1978.8 GPa	$E_3 = 3E_2 + 2(l + 2m)$
Dislocation density	Λ	2.5×10^{15} m/m³[c]	
Conversion factors	g	0.33[c]	
	R	0.33[c]	

[a]Ref. 38.
[b]Ref. 39.
[c]Ref. 40.

Making use of the parameters in Table I, we obtain the intrinsic ANLP $\beta^{lat} = 7.3$ (lattice contribution) and the excess ANLP due to dislocation movement,

$$\beta_0^{dis} = \frac{2E_2^2 g \Lambda k R^2 b_p^3}{\gamma^3} = 6.6,$$

$$\beta_\sigma^{dis} = \frac{6E_2^2 g \Lambda k R^3 b_p^4}{\gamma^4} \sigma_0 = 1.1 \times 10^{-8} \frac{\sigma_0}{N/m^2}. \tag{24}$$

In the above calculations, the angle of inclination ϕ in Fig. 1 is taken to be $\pi/4$. Even if the initial stress is 100 MPa, the stress-dependent part is only $\beta_\sigma^{dis} = 1.1$, which gives the total excess ANLP $\beta^{dis} = \beta_0^{dis} + \beta_\sigma^{dis} = 7.7$.

To close this section, it is worth noting that Eq. (24) gives the dominant terms in the formula of excess ANLP. The order of magnitude analysis used in deriving Eq. (24) is based on material parameters for Ni as listed in Table 3.1. However, the results are applicable to most of the metallic materials, i.e., $\beta^{dis} = \beta_0^{dis} + \beta_\sigma^{dis}$, where

$$\beta_0^{dis} = \frac{2E_2^2 g \Lambda k R^2 b_p^3}{\gamma^3}, \beta_\sigma^{dis} = \frac{6E_2^2 g \Lambda k R^3 b_p^4}{\gamma^4} \sigma_0 \tag{25}$$

provide good approximations when the dislocation density is below $10^{17} m/m^3$.

IV. COMPARISON OF DIFFERENT MODELS ON DISLOCATION-INDUCED ANLP

Substituting Eq. (8) into Eq. (25) in conjunction with Eq. (6) leads to

$$\beta_0^{dis} = \left(\frac{128\pi^2 g R^2}{\eta^2}\right)\left(\frac{E_2}{\mu}\right)^2 (\Lambda b_p^2)\left(\frac{r_e}{b_p}\right)^3,$$

$$\beta_\sigma^{dis} = \left(\frac{3072\pi^3 g R^3}{\eta^3}\right)\left(\frac{E_2}{\mu}\right)^2 \left(\frac{\sigma_0}{\mu}\right)(\Lambda b_p^2)\left(\frac{r_e}{b_p}\right)^4. \tag{26}$$

This represents the ANLP induced by extended dislocations. For brevity, we will call Eq. (26) the extended dislocation model (EDM). For comparison, the EDM is listed in Table II together with expressions of the excess ANLPs given by the dislocation monopole model (DMM) and dislocation dipole model (DDM). Interestingly, all these expressions have very similar form and structure, particularly between dislocation d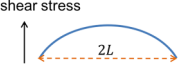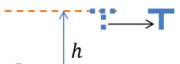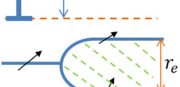ipoles and extended dislocations, although they represent different physics. Monopoles and dipoles are perfect dislocations, while extended dislocations consist of partials and stacking faults.

All three models are based on dislocation glide motion. The DMM considers the bow-out of dislocation strings on slip planes, the DDM describes the relative motion of two nearby edge dislocations on different slip planes, and the EDM accounts for the relative motion of two partial dislocations that enclose a stacking fault on the same slip plane. In DMM and EDM, the dislocations are usually mixed (including both edge and screw components) but the DDM only considers edge dislocations.

We are now in a position to estimate the relative magnitude of the excess ANLPs from these three different crystalline defects. Again, we use Ni as an example, whose material parameters are given in Table 3.1. At room temperature, the average height for edge-dipoles is $h = 4$ nm,[41,42] the segment length L for dislocation monopoles may range from 10 nm to 10^4 nm,[43] and a typical value of L can be taken as 2×10^{-6} m.[15] The magnitude of the Burgers vectors of perfect dislocations for edge-dipoles and monopole is 0.4 nm.[40] Based on these parameters, β_0^{dis} and β_σ^{dis} are plotted in Figs. 3(a) and 3(b), respectively. For comparison, β^{lat} is included in both figures. It is seen from both figures that the excess ANLPs generated by dislocation dipoles and extended dislocations have a similar order of magnitude in that their characteristic lengths are close to each other. But in Fig. 3(b), the effect of dislocation monopoles is dominant. It is approximately seven orders of magnitude higher than the results of the other two kinds of dislocation substructures.

Furthermore, it is seen from their expressions that the excess ANLPs scale with $(L_{char}/b)^n$, where b is the magnitude of Burgers vector and L_{char} is a characteristic length such as the dislocation segment length, dipole height, or the equilibrium distance between the two partials. The exponent n is 3 for the stress-dependent term and 4 for the stress-independent term. The magnitude of the excess ANLP is determined by the ratio L_{char}/b. The magnitude of Burgers vector b is typically in Ångströms (10^{-1} nm). For dislocation dipole and extended dislocations, L_{char} is typically 1–10 nanometers,[42] and thus L_{char}/b is typically in the order of 10–100. But for dislocation monopoles, L_{char} is generally from 10 nm to 10^4 nm,[43] and L_{char}/b is in the order of 1000 if L_{char} is typically around 10^{-6} m.[15] This semi-quantitative

TABLE II. Comparisons of models on the dislocation-induced ANLP.

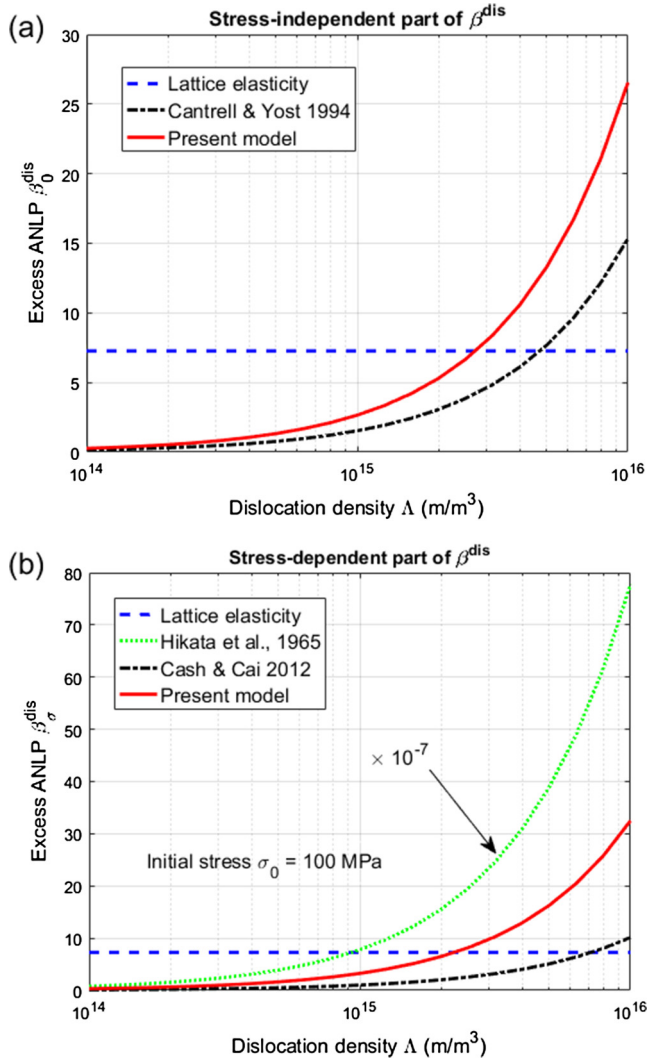| Models	Configurations	Stress-independent β_0^{dis}	Stress-dependent β_σ^{dis}
DMM[a]	shear stress	0	$\left(\frac{24gR^3}{5}\right)\left(\frac{E_2}{\mu}\right)^2\left(\frac{\sigma_0}{\mu}\right)(\Lambda b^2)\left(\frac{L}{b}\right)^4$
DDM[b]		$16\pi^2 g R^2 (1-\nu)^2\left(\frac{E_2}{\mu}\right)^2(\Lambda b^2)\left(\frac{h}{b}\right)^3$	$384\pi^3 g R^3 (1-\nu)^3\left(\frac{E_2}{\mu}\right)^2\left(\frac{\sigma_0}{\mu}\right)(\Lambda b^2)\left(\frac{h}{b}\right)^4$
EDM		$\left(\frac{128\pi^2 g R^2}{\eta^2}\right)\left(\frac{E_2}{\mu}\right)^2(\Lambda b_p^2)\left(\frac{r_e}{b_p}\right)^3$	$\left(\frac{3072\pi^3 g R^3}{\eta^3}\right)\left(\frac{E_2}{\mu}\right)^2\left(\frac{\sigma_0}{\mu}\right)(\Lambda b_p^2)\left(\frac{r_e}{b_p}\right)^4$

[a]Ref. 15.
[b]Refs. 19 and 31.

FIG. 3. Comparison of the excess ANLP β^{dis} predicted by different models: (a) Stress-independent part of the excess ANLP; (b) Stress-dependent part of the excess ANLP with pre-stress $\sigma_0 = 100\,\text{MPa}$. (Result of DMM is multiplied by 1×10^{-7}).
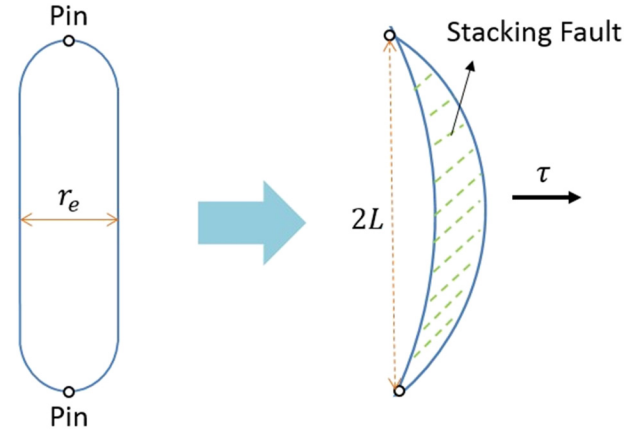

FIG. 4. Segment of extended dislocation pinned in the glide plane.

the vibrational glide motion of dislocation lines induced by the passing elastic waves. This implies that it would be difficult to identify the type of dislocation substructures using the method of second harmonic generation.

In closing, we note that the present model is a simplification of realistic extended dislocations. In real materials, the two partial dislocations are generally not infinitely long and straight. They are typically pinned by precipitates or other defects, see Fig. 4. Under shear stress, both partials will bow out from their equilibrium position, from which an improved model may be developed. This improved model can be regarded as a combination of the DDM and EDM, in which the two partial dislocation segments enclosing the stacking faults are pinned at their ends. Such a configuration was shown in Hirth and Lothe.[32,44] Although it is possible to construct this more realistic model conceptually, deriving it analytically is much more difficult. A numerical solution will be needed. An investigation on this model will be reported in a separate publication.

analysis explains why the effect of dislocation monopoles is much more pronounced than the other two kinds of dislocation substructures under the same density and pre-stress.

V. CONCLUSION

In this paper, an analytical model is developed that quantitatively relates the excess ANLP to the density of extended dislocations and their physical and geometrical characteristics such as stacking fault energy and equilibrium distance between the two partials. Since the ANLP can be measured through ultrasonic tests, this model enables the nondestructive evaluation of extended dislocations.

Further, we found that the mathematical structure of the model is very similar to those of the dislocation monopole and dipole models. They are all scaled with $(L_{char}/b)^n$, where L_{char} is a characteristic length, b is the magnitude of Burgers vector, and n is 3 for the stress-dependent term and 4 for the stress-independent term. This is understandable because, in all three cases, the excess acoustic nonlinearity is caused by

[1] J. Herrmann, J. Y. Kim, L. J. Jacobs, J. M. Qu, J. W. Littles, and M. F. Savage, J. Appl. Phys. **99**(12), 124913 (2006).
[2] J. Y. Kim, L. J. Jacobs, J. M. Qu, and J. W. Littles, J. Acoust. Soc. Am. **120**(3), 1266–1273 (2006).
[3] J. Y. Kim, J. Qu, L. J. Jacobs, J. W. Littles, and M. F. Savage, J. Nondestruct. Eval. **25**(1), 29–37 (2006).
[4] C. Bermes, J. Y. Kim, J. M. Qu, and L. J. Jacobs, Appl. Phys. Lett. **90**(2), 021901 (2007).
[5] C. Pruell, J. Y. Kim, J. Qu, and L. J. Jacobs, Appl. Phys. Lett. **91**(23), 231911 (2007).
[6] C. Bermes, J. Y. Kim, J. M. Qu, and L. J. Jacobs, Mech. Syst. Signal Proc. **22**(3), 638–646 (2008).
[7] G. Shui, J. Y. Kim, J. Qu, Y. S. Wang, and L. J. Jacobs, NDT E Int. **41**(5), 326–329 (2008).
[8] C. Pruell, J. Y. Kim, J. M. Qu, and L. J. Jacobs, Smart Mater. Struct. **18**(3), 035003 (2009).
[9] M. F. Muller, J. Y. Kim, J. M. Qu, and L. J. Jacobs, J. Acoust. Soc. Am. **127**(4), 2141–2152 (2010).
[10] M. H. Liu, J. Y. Kim, L. Jacobs, and J. M. Qu, NDT E Int. **44**(1), 67–74 (2011).
[11] S. V. Walker, J. Y. Kim, J. M. Qu, and L. J. Jacobs, NDT E Int. **48**, 10–15 (2012).

[12]K. Huang, Proc. R. Soc. Lond. A Math. Phys. Sci. **203**(1073), 178 (1950).

[13]J. M. Qu, L. J. Jacobs, and P. B. Nagy, J. Acoust. Soc. Am. **129**(6), 3449–3452 (2011).

[14]J. M. Qu, P. B. Nagy, and L. J. Jacobs, J. Acoust. Soc. Am. **131**(3), 1827–1830 (2012).

[15]A. Hikata, B. B. Chick, and C. Elbaum, J. Appl. Phys. **36**(1), 229–236 (1965).

[16]T. Suzuki, A. Hikata, and C. Elbaum, J. Appl. Phys. **35**(9), 2761–2766 (1964).

[17]Z. Chen and J. Qu, J. Appl. Phys. **114**(16), 164906 (2013).

[18]W. D. Cash and W. Cai, J. Appl. Phys. **109**(1), 014915 (2011).

[19]W. D. Cash and W. Cai, J. Appl. Phys. **111**(7), 074906 (2012).

[20]J. H. Cantrell and W. T. Yost, J. Appl. Phys. **81**(7), 2957–2962 (1997).

[21]J. H. Cantrell and X. G. Zhang, J. Appl. Phys. **84**(10), 5469–5472 (1998).

[22]K. H. Matlack, H. A. Bradley, S. Thiele, J. Y. Kim, J. J. Wall, H. J. Jung, J. M. Qu, and L. J. Jacobs, NDT E Int. **71**, 8–15 (2015).

[23]K. H. Matlack, J. Y. Kim, L. J. Jacobs, and J. Qu, J. Nondestruct. Eval. **34**(1), 273 (2015).

[24]A. L. Matveev, V. E. Nazarov, A. I. Potapov, I. A. Sostova, and A. M. Sutin, Acoust. Phys. **45**(4), 483–487 (1999).

[25]V. E. Nazarov and A. M. Sutin, J. Acoust. Soc. Am. **102**(6), 3349–3354 (1997).

[26]Y. X. Zhao, Y. J. Qiu, L. J. Jacobs, and J. M. Qu, J. Appl. Mech. Trans. ASME **82**(8), 081006 (2015).

[27]Y. X. Zhao, Y. J. Qiu, L. J. Jacobs, and J. M. Qu, Acta Mech. **227**(2), 399–419 (2016).

[28]A. H. Cottrell, Sci. Am. **217**, 90–101 (1967).

[29]K. Teichmann, C. H. Liebscher, R. Volkl, U. Glatzel, and S. Vorberg, Platinum Metals Rev. **55**(4), 217–224 (2011).

[30]S. Suresh, *Fatigue of Materials*, 2nd ed. (Cambridge University Press, Cambridge, 1998).

[31]J. H. Cantrell and W. T. Yost, Philos. Mag. A **69**(2), 315–326 (1994).

[32]J. P. Hirth and J. Lothe, *Theory of Dislocations*, 2nd ed. (Wiley, New York, 1982).

[33]D. Hull and D. J. Bacon, *Introduction to Dislocations*, 5th ed. (Butterworth-Heinemann, Elsevier, 2011).

[34]T. S. Byun, Acta Mater. **51**(11), 3063–3071 (2003).

[35]J. Weertman and J. R. Weertman, *Elementary Dislocation Theory* (Macmillan, New York, 1964).

[36]W. T. Read, *Dislocations in Crystals* (McGraw-Hill, New York, 1953).

[37]M. Peach and J. S. Koehler, Phys. Rev. **80**(3), 436–439 (1950).

[38]P. Haasen, Philos. Mag. **3**(28), 384–418 (1958).

[39]D. I. Crecraft, J. Sound Vib. **5**(1), 173–192 (1967).

[40]J. H. Cantrell and W. T. Yost, Int. J. Fatigue **23**, 487–490 (2001).

[41]B. Tippelt, Philos. Mag. Lett. **74**(3), 161–166 (1996).

[42]M. E. Kassner and M. A. Wall, Metall. Mater. Trans. A **30**(13), 777–779 (1999).

[43]A. Granato and K. Lücke, J. Appl. Phys. **27**(6), 583–593 (1956).

[44]T. Malis, D. J. Lloyd, and K. Tangri, Metall. Trans. A **6**(4), 932 (1975).